

PBBFMM3D: a Parallel Black-Box Fast Multipole Method for Non-oscillatory Kernels

Ruoxi Wang^a, Chao Chen^a, Jonghyun Lee^b, Eric Darve^{a,c}

^a*Institute for Computational and Mathematical Engineering, Stanford University*

^b*Water Resources Research Center, Department of Civil and Environmental Engineering,
University of Hawaii*

^c*Department of Mechanical Engineering, Stanford University*

Abstract

This paper presents PBBFMM3D: a parallel black-box fast multipole method that accelerates kernel matrix-vector multiplications where the kernel is a non-oscillatory function in three dimensions. Such problems arise from a wide range of fields, *e.g.*, computational mechanics, geosciences and machine learning. While a naive direct evaluation has an $O(N^2)$ complexity in time and storage, which is prohibitive for large-scale applications, PBBFMM3D reduces the costs to $O(N)$. In contrast to other fast methods that require the knowledge of the explicit kernel formula, PBBFMM3D requires only the ability to evaluate the kernel. To further accelerate the computation on shared-memory machines, the parallelism in PBBFMM3D was analyzed and implemented using OpenMP. We show numerical experiments on the accuracy and the parallel scalability of PBBFMM3D, as well as its applications to covariance matrix computations that are heavily used in parameter estimation techniques, such as kriging and Kalman filtering.

Keywords: fast multipole method, shared-memory parallelism, particle simulation, covariance matrix

1. Motivation and significance

We consider the problem of computing kernel matrix-vector products, where the kernel function is non-oscillatory and sufficiently smooth away from the origin. The problem can be formulated mathematically as the following.

Email addresses: ruoxi.rw@gmail.com (Ruoxi Wang), chenchao.nk@gmail.com (Chao Chen), jonghyun.harry.lee@hawaii.edu (Jonghyun Lee), darve@stanford.edu (Eric Darve)

$$\phi_i = \sum_{j=1}^N \mathcal{K}(\mathbf{x}_i, \mathbf{y}_j) \sigma_j, \quad i = 1, \dots, N \quad (1)$$

where \mathcal{K} is a kernel function, $\{\mathbf{x}_i\}_{i=1}^N$ and $\{\mathbf{y}_i\}_{i=1}^N$ are data points in a three-dimensional space, and σ_i is the weight associates with \mathbf{y}_i . The matrix form of Eq. (1) is $\boldsymbol{\phi} = \mathbf{K}\boldsymbol{\sigma}$, where $\mathbf{K}_{ij} = \mathcal{K}(\mathbf{x}_i, \mathbf{x}_j)$ and

$$\boldsymbol{\sigma} = [\sigma_1, \dots, \sigma_n]^T, \quad \boldsymbol{\phi} = [\phi_1, \dots, \phi_n]^T.$$

Throughout the paper, we refer to the problem in Eq. (1) as a matrix-vector multiplication.

Dense matrix operations (Eq. (1)) occur in a broad spectrum of applications in science and engineering. Some classic applications include particle simulations [1], numerical partial differential equations (*e.g.*, boundary element methods [2]), and material science (*e.g.*, dislocation dynamics simulations [3]). There are also applications in geostatistics, including *e.g.*, Kalman filters, inverse problems in hydro-geology and petroleum engineering [2]. Moreover, in the field of machine learning, these matrix operations are critical components in kernel methods [4, 5], as well as the *t*-Distributed Stochastic Neighbor Embedding (*t*-SNE) algorithm.

For a problem of size N (number of particles), a direct calculation of all the pair-wise interactions requires $O(N^2)$ memory and computation time, which is prohibitive for large-scale applications. The fast multipole method (FMM) reduces the cost down to $O(N)$.

The fundamental idea of FMM is to separate the interactions into near-field and far-field interactions, where the near-field interactions are computed exactly, and the far-field interactions are approximated using low-rank techniques. The original FMM [1] was introduced for particle simulations and is based on the spherical harmonics expansion of the Laplace kernel. Although the FMM was extended to other kernels frequently used in PDEs [6, 7, 8, 9], derivations are required for a new kernel, making existing software codes no longer applicable. Moreover, in many cases, the derivations are difficult or even impossible for a complicated kernel that may not have a closed analytic form. To address these problems, we have implemented a parallel black-box fast multipole method in three dimensions (PBBFMM3D) based on the kernel-independent FMM in [10, 3]. **Our method requires only numerical evaluations of the kernel function and provides a black-box interface to users.**

One significant feature of PBBFMM3D is that it applies to all non-oscillatory smooth kernels, which is a feature that some of the other packages lack. In addition, it offers two options for approximating the far-field

interactions, making the package efficient for all accuracy levels. One option uses **Chebyshev interpolants**, which is known to be nearly optimal [11]. The other option uses **Lagrange interpolants on uniform grids**, which leads to a block-Toeplitz structure of the translation operators and enables the usage of the fast Fourier transform (FFT). Many papers [3, 2, 12, 13] report a significant acceleration using our code which is available at <https://github.com/ruoxi-wang/PBBFMM3D>.

1.1. Related work

An important part that differentiates FMM methods is the low-rank operators for approximating far-field interactions. The original FMM [1] is based on spherical harmonics expansions of the Laplace kernel. Using this approach leads to difficulties each time a new kernel is used and limits the types of problems that can be solved. The kernel-independent FMMs, on the other hand, require only numerical kernel evaluations on data points and can be applied to more general problems.

Several methods to construct kernel-independent FMMs are available. One popular approach is to approximate the kernel functions by polynomials, which has an advantage that it applies to non-oscillatory kernels that are sufficiently smooth away from their singularities. The resulting operators are then compressed by the singular value decomposition (SVD) to accelerate the running time. Examples of this approach are in [14, 15, 10]. Another line of work computes equivalent densities [16, 17, 18] by making indirect use of analytical expansions of the kernel function. There has also been work using fast algebraic techniques. Examples include the interpolative decomposition (ID) [19, 20] and adaptive cross approximations (ACA) [21].

1.2. Main contributions

We present a parallel implementation of the kernel independent FMM described in [10]. It computes the matrix-vector multiplication in Eq. (1) in $O(N)$. The following lists some main features of our package and specifically, our package

- applies to all non-oscillatory smooth kernels and only requires the kernel’s numerical evaluation at data points. In this paper, “smooth” means that relatively low order polynomials can provide a good approximation of the kernel in some suitable interval away from zero.
- is parallelized with OpenMP for shared memory machines.
- is efficient for both low and high accuracies (a choice of Chebyshev and uniform interpolations).

- pre-computes and compresses far-field translation operators.
- applies to multiple sets of weights in one pass.

This paper is organized as follows. Section 2 describes the kernel-independent FMM algorithm implemented. Section 3 describes the architecture and functionalities of our software. Section 4 demonstrates the performance in terms of the computational cost, convergence and parallel scalability. Some applications are also shown.

2. Algorithm

This section describes the black-box fast multipole method (BBFMM) [10] in three dimensions. The algorithm divides the interactions into near-field and far-field interactions, where the near-field interactions are computed exactly, and the far-field interactions are approximated using a hierarchical low-rank structure. The first step of the algorithm is to recursively divide the 3D domain using an octree until each leaf cell contains a constant number of data points. For illustration purpose, throughout this section, we use a binary tree and quadtree.

For each cell \mathcal{C} , its potential is computed by summing over the interactions with three types of cells (depicted in Figure 1): the neighbors of \mathcal{C} , the interaction list of \mathcal{C} and the remaining cells. The interactions with neighboring cells are computed exactly and with all the other cells are computed using low-rank techniques.

Kernel independence. The low-rank methods used in the algorithm has the following analytic form

$$\mathcal{K}(\mathbf{x}, \mathbf{y}) = \sum_i \sum_j L_p(\mathbf{x}, \mathbf{x}_i^*) \mathcal{K}(\mathbf{x}_i^*, \mathbf{y}_j^*) L_p(\mathbf{y}_j^*, \mathbf{y}), \quad (2)$$

where L_p is an interpolation operator of degree p , and \mathbf{x}_i^* and \mathbf{y}_j^* are interpolation points. Eq. 2 only requires evaluations of kernels at the data points, making the algorithm appealing to a wide range of kernels.

Interpolation schemes. Two types of interpolation operators are used in the algorithm: Chebyshev polynomials and Lagrange basis polynomials. The Chebyshev polynomials are near-optimal in terms of accuracy. The Lagrange basis polynomials can significantly accelerate the computations of the $M2L$ operators. They are based on uniform grids, which enables the use of FFT and reduces the computation and memory from $O(p^6)$ to $O(p^3)$, where p is the interpolation order. Detailed comparisons between these two schemes are in Section 4.

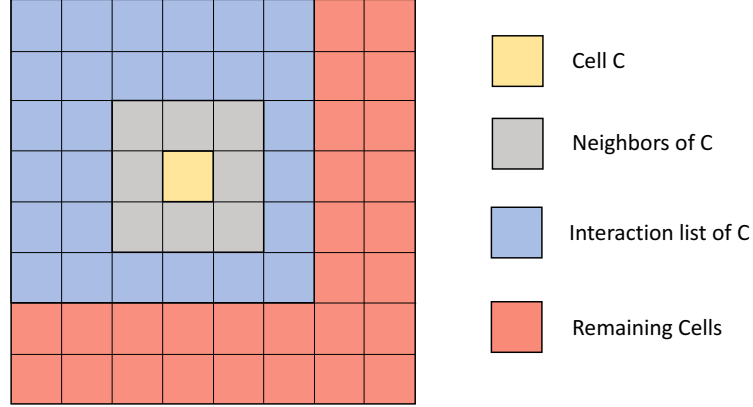


Figure 1: Cells at level 3 of a quad tree.

FMM translation operators. We first introduce the five (standard) FMM translation operators that are key components of the algorithm. We will use the standard FMM terminologies such as multipole expansion and local expansion (see [1] for rigorous definitions).

- *Particle to Moment (P2M).* For every leaf cell, compute its multipole expansion from the source points in the cell.
- *Moment to Moment (M2M).* For every non-leaf cell, compute its multipole expansion based on the multipole expansions of all its children.
- *Moment to Local (M2L).* For every cell, compute its local expansion based on the multipole expansions of the cells in its interaction list.
- *Local to Local (L2L).* For every cell, add contributions to its local expansion from the local expansion of its parent.
- *Local to Particle (L2P).* For every leaf cell, compute the far-field interactions on the target points from the cell's local expansion.

Having introduced the translation operators, we demonstrate the computation through an 1D example in Figure 2. For neighbors, the interactions are computed exactly; for cells in the interaction list, the interactions are approximated by low-rank methods; and for the remaining cells, the interactions are approximated through coarser (upper) levels in the tree.

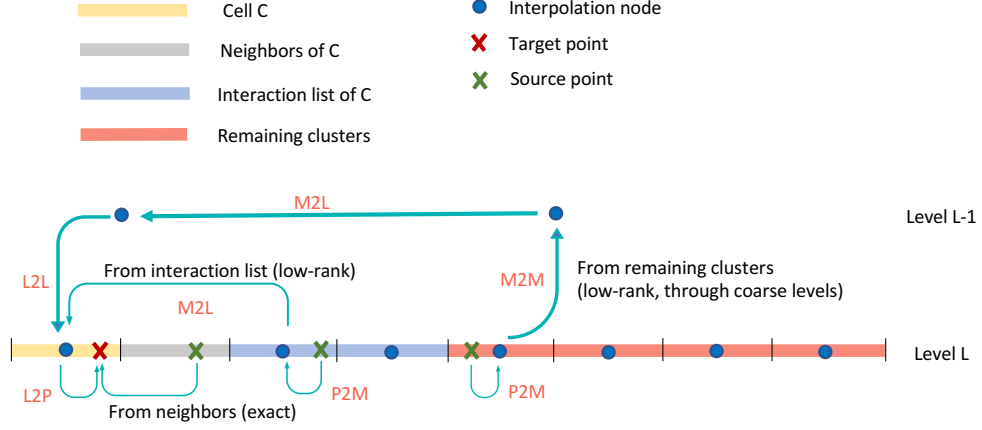


Figure 2: Potential calculation of a leaf cell in a binary tree (1D case). In the figure, parts of two levels in the tree are shown for simplicity. Red/green cross represents the target/source point; blue dots represent the interpolation nodes; arrows represent the flow of contributions of potential. $M2M$, $M2L$, $L2L$, $L2P$ and $P2M$ are translation operators. For each cell type, the translation operators are shown for only one cell for simplicity.

FMM algorithm. Finally, we describe the FMM algorithm. The main algorithm consists of four stages with the first three stages depicted in Figure 3 using a quadtree (2D case). Details of the four stages are described in the following.

1. *Upward Pass.* This stage first applies the $P2M$ translations to the leaf cells, and then applies the $M2M$ translations to the non-leaf cells through a bottom-up tree traversal, which encodes the source information to upper-level cells.
2. *Far-field interaction.* The $M2L$ translations are applied to all the cells, which efficiently computes the potential contributed from far-field points, and stores the information in local expansions. This stage can be applied simultaneously to all the cells in the tree.
3. *Downward Pass.* After the $M2L$ translations are computed, the $L2L$ translations are applied to the non-leaf cells through a top-down tree traversal, which translates local expansions hierarchically down to the leaf nodes. Then, the $L2P$ translations are applied to each leaf cell.
4. *Near-field interaction.* Finally, each target point in the leaf node adds the near-field contributions from the neighboring source points to its

potential. This stage can also be applied simultaneously to all the leaf cells.

Our implementation follows the flow of the above-described algorithm and each stage has further been parallelized (see Section 3.1.1).

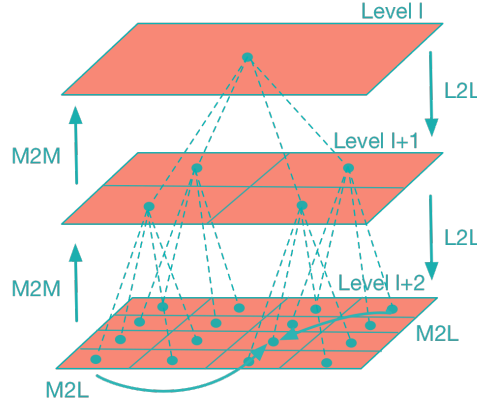


Figure 3: A three-level decomposition of a 2D domain and three translation operators in the FMM. In the upward pass, $M2M$ translations are computed using a bottom-up tree traversal, passing the information from children to the parent (dashed lines). In far-field translations, $M2L$ operators are applied on each cell, and the information is gathered from interaction lists (curved arrows). In the downward pass, $L2L$ translations are computed using a top-down tree traversal, passing the information from parents to children (dashed lines).

3. Software description.

PBBFMM3D is a parallel implementation of the BBFMM in three dimensions, which calculates a matrix-vector product of the form Eq. (1) in $O(N)$ complexity. PBBFMM3D is an open-source software package which can be redistributed and/or modified under the terms of the Mozilla Public License (MPL2) license¹. It requires the FFTW² library and the OpenMP compiler. It was written in C/C++ and offers a Python interface. The package can be downloaded from <https://github.com/ruoxi-wang/PBBFMM3D>. The architecture and implementation details are described in Section 3.1, and the functionalities are introduced in Section 3.2.

¹<https://www.mozilla.org/en-US/MPL/2.0/>

²<http://www.fftw.org/>

3.1. Software Architecture

The software repository has the following three main classes as shown in Figure 4.

Class **H2_2D_Tree** stores the information regarding the tree structure, the requested accuracy, and the type of interpolation scheme. **PrecomputeM2L()** pre-computes the *M2L* operator and stores the compressed matrices for later calculations, and **BuildFMMHierarchy()** builds the tree recursively.

Class **H2_2D_Compute** stores the information regarding the data points \mathbf{x}_i , \mathbf{y}_i and weights σ_i . It contains five key functions where four of them correspond to the four translation stages described in Section 2. Specifically, **FMMDistribute()** distributes the source and the target points to leaf cells in the FMM tree and sets up the interaction list for each cell. **UpwardPass()** first computes *P2M* for leaf cells and then computes *M2M* for each non-leaf cell through a bottom-up tree traversal. **FarFieldInteractions()** applies the *M2L* operators to all cells. **DownwardPass()** first applies *L2L* using a top-down tree traversal and then applies *L2P* to all the leaves. Finally, **NearFieldInteractions()** computes the exact contribution from neighboring cells.

Class **kernel_NAME** inherits from class **H2_2D_Tree** and defines the kernel function. Function **SetKernelProperty()** sets the homogeneous and symmetric property of a kernel. Function **EvaluateKernel()** takes two data points \mathbf{x} and \mathbf{y} and returns the value of $\mathcal{K}(\mathbf{x}, \mathbf{y})$. This function reflects the kernel-independent nature of the PBBFMM3D package.

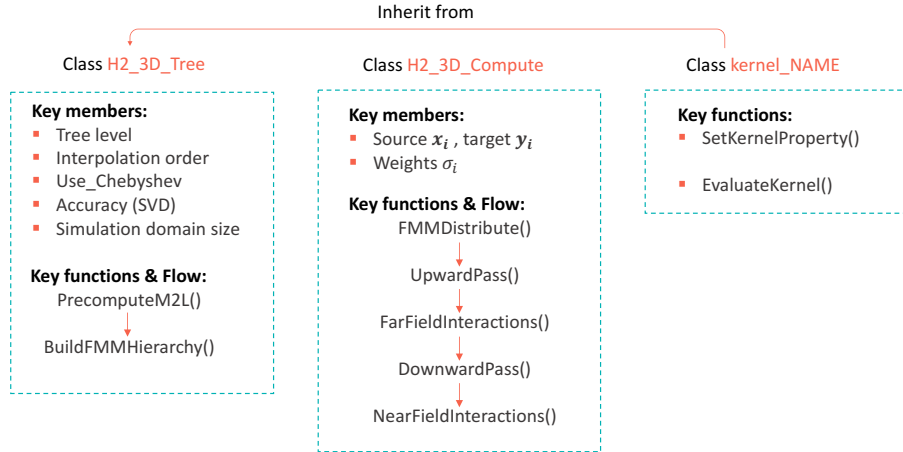


Figure 4: Classes with their key members and functions. The three columns list three classes with their inheritance relationship. The arrow represents the flow of the algorithm.

3.1.1. Parallelization using OpenMP

This section describes the parallelization details using OpenMP for shared-memory machines. Our FMM code used a balanced oct-tree structure. Although an adaptive tree structure extends to more general cases, our balanced tree structure works well because in practice, most data distributions are not extremely non-uniform. This design choice also leads to a much easier parallel implementation as discussed below. We focus our discussion on the parallelization of the four FMM stages: upward pass, far-field interactions, downward pass and near-field interactions.

In the upward pass, the computation for the parent depends on its children. Hence, we performed a bottom-up tree traversal in a level-to-level fashion, and within each level, the computations were carried out in parallel over all the cells using a “parallel for”. The downward pass, which is symmetric to the upward pass, used a similar parallel tree traversal method. For far-field (near-field) interactions, the computations for all the cells (leaves) are independent of other cells. Therefore, a massive parallelization using “parallel for” was applied.

A task-based tree traversal is in principle the optimal parallel strategy but it involves more runtime overhead than our simple level-by-level traversal. In practice, we found similar performance between these two strategies in our experiments.

Further optimization can be carried out by exploring the explicit dependency of these four stages. For example, the $M2L$ translation of a cell could start immediately after the $M2M$ translations of cells in its interaction list have completed. See [22, 23] for a task-based approach.

3.1.2. Performance optimizations

We discuss some optimizations implemented for performance improvements.

Symmetric matrix. Many operations can be saved by taking advantage of the symmetric property. For two cells \mathcal{C}_1 and \mathcal{C}_2 that are either neighbors or in each other’s interaction list, only one of the two interaction matrices is constructed, say $\mathcal{K}(\mathcal{C}_1, \mathcal{C}_2)$, and the other is applied using the transpose of $\mathcal{K}(\mathcal{C}_1, \mathcal{C}_2)$. Further, for each leaf cell \mathcal{C} , the self-interaction matrix $\mathcal{K}(\mathcal{C}, \mathcal{C})$ is evaluated for only the upper triangular part.

Applying to multiple sets of weights (vectors). Applying a kernel matrix to a set of vectors is common in practice, *e.g.*, randomized SVDs. In such case, the computations for all the vectors are carried out in one pass, which allows

the use of cache-friendly BLAS3³ matrix operations.

Homogeneous kernels. For homogeneous kernels

$$\mathcal{K}(\alpha \mathbf{x}, \alpha \mathbf{y}) = \alpha^m \mathcal{K}(\mathbf{x}, \mathbf{y})$$

the *M2L* computations can be significantly accelerated because we only need to compute the operators in one level.

Uniform interpolations. The *M2L* operators have nested-Toeplitz structure [3], to which the FFT can be applied for fast translations.

3.2. Software Functionalities

This section presents the functionalities of our software. An overview is in Table 1 which lists the main functionality, the advantages and some applications.

Table 1: Software overview.

Basic functionalities	
Input:	[problem] data $\{\mathbf{x}_i\}_{i=1}^N$, $\{\mathbf{y}_i\}_{i=1}^N$; weights $\{\sigma_i\}_{i=1}^N$; kernel \mathcal{K} [accuracy] interpolation order [time & memory] SVD accuracy; tree level
Output:	Approximation of $\sum_{j=1}^N \mathcal{K}(x_i, x_j) \sigma_j$, $\forall i$
Complexity:	$O(N)$
Programming languages	Interfaces
C/C++, OpenMP	C++, Python
Advantages	
<ul style="list-style-type: none"> – applies to all non-oscillatory smooth kernels (<i>e.g.</i>, $\exp(-r^2)$, $\frac{1}{r}$, $\log(r)$) – is efficient for both low and high accuracies (two interpolation scheme options) – pre-computes and compresses the <i>M2L</i> factors – is parallelized with OpenMP – applies to multiple vectors in one pass – is efficient for homogeneous kernels 	
Applications	
Particle potential evaluations; dislocation dynamics simulations; inverse modeling and Kalman filters; data visualizations (t-SNE)	

³http://www.netlib.org/blas/#_level_3

In the following, we briefly describe the basic usage, customized kernels, and the Python interface. For further details of the package, we refer to readers the documentation in <https://github.com/ruoxi-wang/PBBFMM3D>.

Basic usage. We demonstrate an example usage of our code in Figure 5. The class `kernel_Gaussian` inherits from class `H2_3D_Tree` and defines the Gaussian kernel. The core part of the calling code only involves three lines. The first two lines construct the tree and pre-compute the $M2L$ operators (if needed). The last line does the rest and outputs the results.

```
// pre-computation
kernel_Gaussian Atree(L, tree_level, interpolation_order, eps,
                      use_chebyshev);
Atree.buildFMMTree();
// computation
H2_3D_Compute<kernel_Gaussian> compute(Atree, target, source,
                                       weight, nCols, output);
```

Figure 5: Basic usage of the PBBFMM3D package. Most input parameters are self-explanatory. L : simulation cell length; ϵ : prescribed SVD accuracy; `use_chebyshev`: 1 for Chebyshev interpolation and 0 for uniform interpolation; `target/source`: input data points; `nCols`: the number of columns of weights.

Customized kernels. This package already offers a wide range of popular kernels for users’ convenience. For customized kernels, the package provides a simple interface to define the kernel function. The user needs to provide the kernel definition and the kernel’s homogeneous and symmetric properties. Figure 6 shows the interface that defines the $\frac{1}{r}$ kernel. The interface is the only part of the source code that users need to modify, and the rest can be seen as a black box.

Interfaces. The code was written in C/C++ for high performance, and was further accelerated by using OpenMP in a multi-core environment. On top of this, we have provided a Python interface for data-science related applications. The interface was implemented using the Boost Python Library. Running the Makefile will generate two libraries (`FMMTree.so` and `FMMCompute.so`). Figure 7 shows a code snippet.

4. Illustrative Examples

This section demonstrates the performance of our software. All the experiments were performed on a workstation with Intel Xeon CPU E5-2699 running at 2.30GHz (36 cores) and 196 GB memory. We used FFTW⁴ and

⁴<http://www.fftw.org/>

```

class myKernel: public H2_3D_Tree {
public:
    myKernel(double L, int tree_level, int interpolation_order,
              double eps, int use_chebyshev):
        H2_3D_Tree(L, tree_level, interpolation_order, eps, use_chebyshev){};
    virtual void SetKernelProperty() {
        homogen = 0;
        symmetry = 1;
        kernelType = "myKernel";
    }
    virtual double EvaluateKernel(vector3& target, vector3& source) {
        vector3 diff;
        diff.x = source.x - field.x;
        diff.y = source.y - field.y;
        diff.z = source.z - field.z;
        double r = sqrt(diff.x*diff.x + diff.y*diff.y + diff.z*diff.z);
        return exp(-r);
    }
};

```

Figure 6: Interface for user defined kernel. The homogeneous indicator `homogen` is 0 for inhomogeneous kernels and m if $\mathcal{K}(\alpha x, \alpha y) = \alpha^m \mathcal{K}(\mathbf{x}, \mathbf{y})$. The symmetric indicator `symmetry` is 0, 1, and -1 for non-symmetric, symmetric, and anti-symmetric ($\mathcal{K}(\alpha \mathbf{x}, \alpha \mathbf{y}) = -\mathcal{K}(\alpha \mathbf{y}, \alpha \mathbf{x})$) kernels, respectively.

```

from FMMTree import *
from FMMCompute import *

myTree = myKernel(L, tree_level, interpolation_order, eps, use_chebyshev)
myTree.buildFMMTree()
Compute(myTree, target, source, weight, nCols, output)

```

Figure 7: Python interface. The input parameters are self-explanatory. The first two lines of the code builds the FMM tree and the last line does the rest of the computations.

Intel MKL⁵ libraries. Section 4.1 shows the computational time and memory, the convergence and parallel scalability. Section 4.2 shows an application in geostatistics.

4.1. Algorithm performance

In this section, we benchmark the performance of our PBBFMM3D package. Section 4.1.1 reports the memory footprint and time results. Section 4.1.2 verifies the convergence of the algorithm. Finally, Section 4.1.3 shows the parallel scalability. All the experiments were run on a single core except for Section 4.1.3, which was run in a multi-core environment. For the Chebyshev interpolation, the compression rate of SVD was selected to be optimal, *i.e.*, the largest value under which the approximation error remains unchanged. The input data were uniformly randomly generated in a unit cube.

Before presenting the experimental results, we first provide some guidance in parameter selection. For interpolation order p , a higher p improves the accuracy but also increases the runtime and memory. For the interpolation scheme, when a low accuracy is requested, Chebyshev scheme is more efficient; when a high accuracy is requested, the uniform scheme is more efficient. For the tree levels, it is often chosen such that the leaf node contains approximately 60 points. For the prescribed accuracy of SVD, it is chosen to be similar to the requested approximation accuracy.

4.1.1. Computational time and memory

We examine the computational time and the memory usage of our software. The computational time is a function of the problem size N , the interpolation order p and the tree level. We focus our study on the first two factors, and chose the tree level such that each leaf cell has approximately 60 points. In the following, we first analyze the complexity of our algorithm and then present some experimental verification.

For an interpolation order p , there are p^3 interpolation nodes in each cell. Therefore, for Chebyshev interpolation, the time complexity is $O(p^9)$ (from SVD compression) for the pre-computation part, and $O(p^6)$ (from matrix multiplications) for the computation part. The memory is dominated by the $M2L$ operators that are generated and stored. Hence, the memory complexity is $O(p^6)$. We can reduce the time and memory by compressing the matrices through an SVD. For uniform interpolation, the time and memory complexity of both pre-computation and computation are $O(p^3 \log(p))$ due to the usage of the FFT.

⁵<https://software.intel.com/en-us/mkl>

Figure 8 shows the runtime vs. the interpolation order p for Chebyshev and uniform interpolations. Subplot (a) shows the pre-computation time and subplot (b) shows the computation time; their sum is the total time. Each p sets an approximation error, and for the same p , the error is roughly the same for both interpolation schemes. The growth rates shown in the plots are consistent with theoretical estimates. In terms of total time, we observe from Figure 8 that in the small p regime ($p \leq 4$, low accuracy), using Chebyshev interpolation is faster; in the large p regime ($p > 4$, high accuracy), uniform interpolation becomes significantly more efficient.

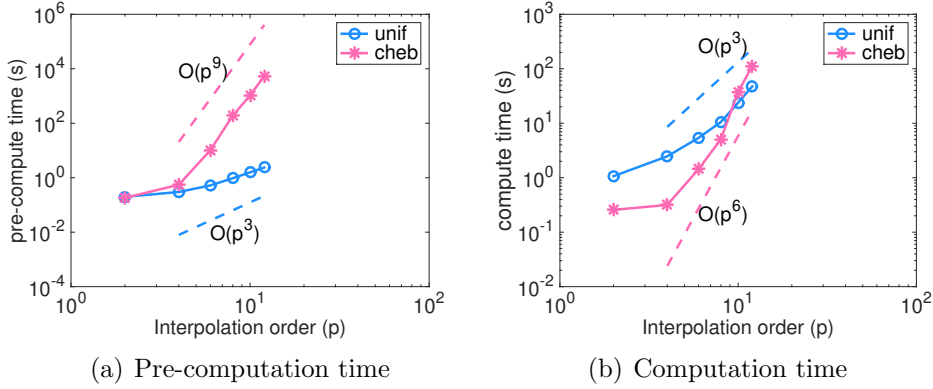


Figure 8: Time vs. interpolation order. The problem size (number of points) and the tree level was fixed at 10^4 and 4, respectively. The kernel used is $\exp(-r)$. The legend represents the interpolation schemes: “unif” means uniform interpolation and “cheb” means Chebyshev interpolation. As the interpolation order p increases, the time for the uniform scheme grows slower than that for the Chebyshev scheme.

Figure 9 verifies the linear scalability with respect to the number of points (problem size). We see that the growth rates for both interpolation schemes are linear, as opposed to the quadratic complexity from a direct calculation.

Figure 10 shows the memory complexity of Chebyshev and uniform interpolations. We see that the complexity shown is consistent with the theoretical complexity, and using the uniform interpolation has significantly reduced the storage.

4.1.2. Convergence

We verify the convergence property of our software. Figure 11 shows the relative error vs. the interpolation order p . The relative error is computed as

$$\frac{\|\hat{K}\mathbf{x} - K\mathbf{x}\|_2}{\|K\mathbf{x}\|_2}$$

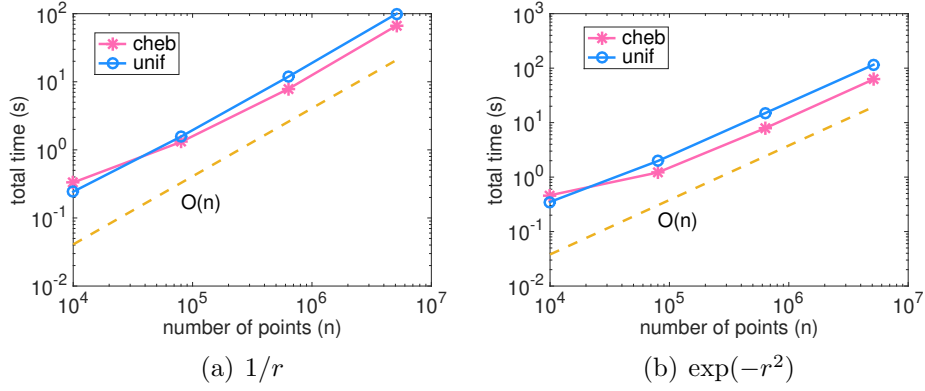


Figure 9: Total time vs. number of points. For each interpolation scheme, the tree level was selected to be 3, 4, 5, 6 for $n = 8^0 \times 10^4, 8^1 \times 10^4, 8^2 \times 10^4, 8^3 \times 10^4$, respectively. The interpolation order was fixed at 4.

where \hat{K} is the approximation matrix and K is the exact matrix. We observe a geometric convergence rate with respect to p for both interpolation methods. The convergence rate for kernel $\exp(-r)$ is $O(10^{-p})$, faster than the $O(5^{-p})$ rate for kernel $1/r$.

4.1.3. Parallel scalability

We demonstrate the parallel scalability of our software. The parallel implementation utilized OpenMP for shared memory machines. The experiments were run with up to 32 cores/threads. For these experiments, we used Chebyshev interpolation and kernel $1/r$; uniform interpolation and other kernel functions provided similar scaling results.

Table 2 reports the total time (excluding pre-computation time) for varying number of cores. We see that the total time decreases as more cores are used. Specifically, for the problem of size $8^4 \times 10^4$, the runtime was accelerated by 19x with 32 cores.

Figure 12 shows the strong scaling for each stage of the FMM as the number of cores increases. We provided a breakdown of the running time for different stages: upward pass, downward pass, far-field interaction, and near-field interaction. We see that the running time for all the stages nearly halved as the number of cores doubled.

Figure 13 shows the weak scalability result. We increased the number of particles proportionally to the number of cores. As the figure shows, the time spent on each stage in the FMM only increased by a small amount when the problem size increased by 8x (the number of cores also increased by 8x). The ideal runtime would stay unchanged due to the linear complexity of FMM.

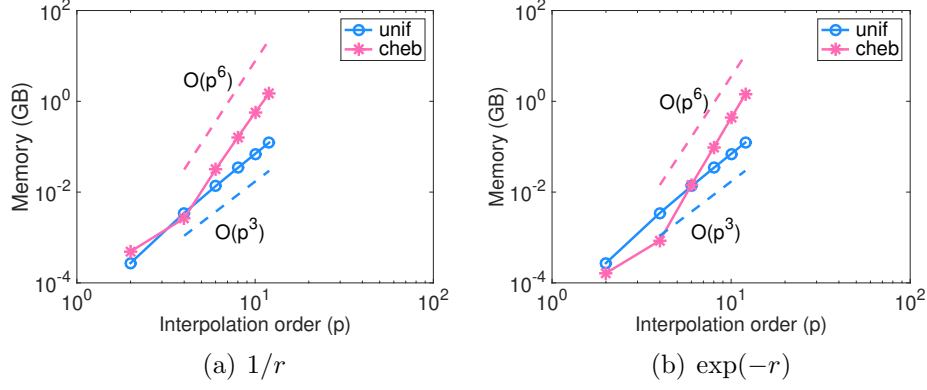


Figure 10: Memory footprint vs. interpolation order p . The number of points was fixed at 10^4 .

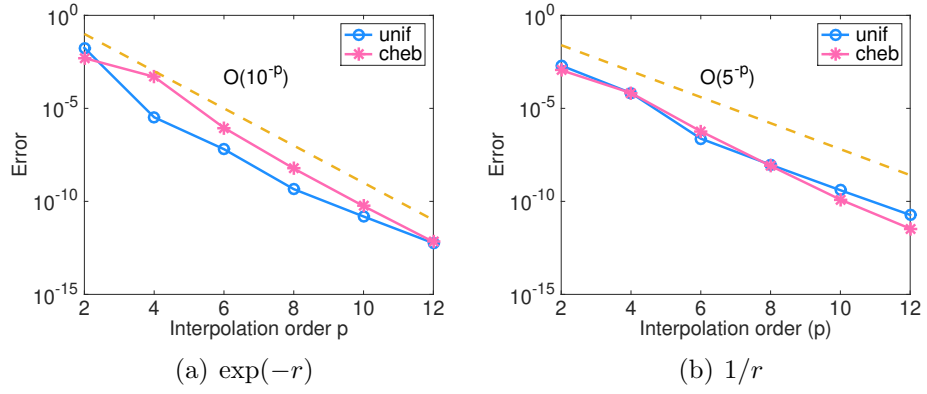


Figure 11: Relative error vs. interpolation order p . The number of points and the number of levels were fixed at 10^4 and 5, respectively. The results converge geometrically with respect to the interpolation order p .

Table 2: Parallel scalability. The kernel used was $1/r$. The Chebyshev interpolation order was fixed at 4. The number of tree levels was selected to be 5, 6, 7 for $n = 8^2 \times 10^4$, $8^3 \times 10^4$ and $8^4 \times 10^4$, respectively. The error was 2.10×10^{-5} , 2.08×10^{-5} , and 2.10×10^{-5} , respectively.

# Points	Time (s)					
	1 core	2 cores	4 cores	8 cores	16 cores	32 cores
$8^2\text{E}+4$	5.74E+0	3.32E+0	1.83E+0	9.93E-1	5.84E-1	4.44E-1
$8^3\text{E}+4$	4.72E+1	2.58E+1	1.40E+1	7.87E+0	4.40E+0	3.49E+0
$8^4\text{E}+4$	4.04E+2	2.15E+2	1.14E+2	6.37E+1	3.72E+1	2.13E+1

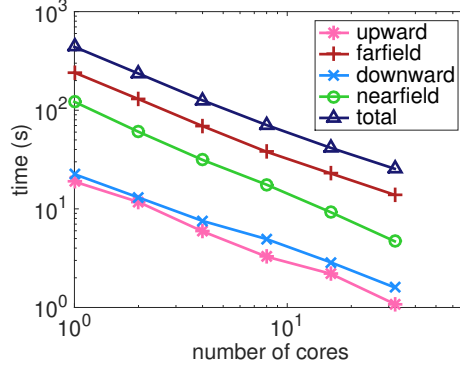


Figure 12: Strong scalability results. The problem size was fixed at $8^4 \times 10^4$. The legend represents four functions: “upward” is the UpwardPass(); “downward” is the DownwardPass(); “farfield” is the FarFieldInteractions(); “nearfield” is the NearFieldInteractions(). The total time is the summation of the four functions and the point distribution time.

Our implementation achieved an efficiency of 73% (serial time/parallel time).

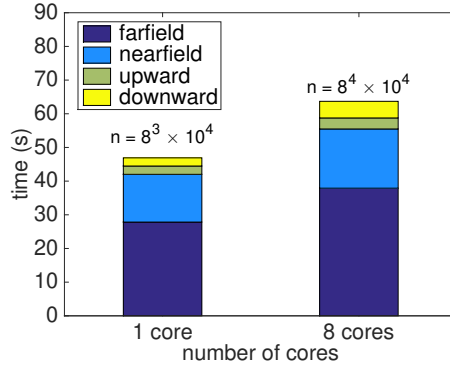


Figure 13: Weak scalability results. The left bar used $8^3 \times 10^4$ points and 1 core; the right bar used $8^4 \times 10^4$ points and 8 cores. The legend represents four functions in the computation.

To summarize, the PBBFMM3D is a parallel package that computes matrix-vector multiplications of the form Eq. 1 in linear complexity. Increasing the interpolation order improves the accuracy but also increases the runtime and memory. For practical use, we recommend the following strategy to choose the interpolation scheme. When a relatively low accuracy is requested ($\approx 10^{-5}$), Chebyshev interpolation is more efficient. When requesting a high accuracy, uniform interpolation is typically more efficient.

4.2. Applications

This section presents some applications of our software. Our software has seen many successful applications. Chen [3] showed that the dislocation dynamics simulations could be significantly accelerated with our code. Simpson [2] adapted our software and accelerated the far-field computations in an isogeometric boundary element method. Lee [12] used our software to speed up large-scale aquifer characterization. In the following, we describe in detail an application in geostatistics.

Gaussian random field (GRF) theory [24, 25] has been widely used in interpolation and estimation of spatially correlated unknowns. For example, estimating permeability of underground soil and rock is of critical interest for hydrogeologists and petroleum engineers [26, 27]. GRF requires a covariance matrix as prior information of underlying unknown fields such as smoothness and uncertainty. Due to the large problem size encountered in practical applications, dimension reduction of the prior matrix through eigenvalue decomposition has been investigated [28, 29, 30].

We compute the truncated eigenvalue decomposition of dense covariance matrices using the randomized SVD (see Algo. 5.3 in [31]) accelerated by PBBFMM3D. The computational cost for a randomized SVD to calculate the top k eigenvalues is $O(N^2k)$, and using PBBFMM3D for matrix operations reduces the cost to $O(Nk)$.

Table 3 reports the timing and accuracy for eigenvalue computations using randomized SVD (randSVD) accelerated by PBBFMM3D. We used an isotropic exponential covariance kernel $\exp(-r)$ and generated the data randomly in a unit cube. We see that PBBFMM3D leads to significant speed gains while maintaining a high accuracy. Further, when the problem size increases to 64×10^4 , randSVD with an exact (direct) matrix computation has reached the memory limit.

Table 3: Time for randomized SVD (randSVD) with exact and PBBFMM3D accelerated matrix multiplications. The requested rank and oversample parameter for randSVD was set to 100 and 20, respectively. The tree level for $n = 10^4, 8 \times 10^4, 64 \times 10^4$ was 3, 4, 5, respectively. The interpolation order was set to 4 and the SVD accuracy was set to 10^{-5} . The error was computed as $\|\Lambda_{fmm} - \Lambda_{ext}\|/\|\Lambda_{ext}\|$ for the top 100 eigenvalues.

# Points	Time (s)		Speedup	Error
	PBBFMM3D	Exact		
10^4	1.30	19.1	15 X	1.6×10^{-4}
8×10^4	9.87	2139	217 X	2.8×10^{-5}
64×10^4	79.6	N/A	N/A	N/A

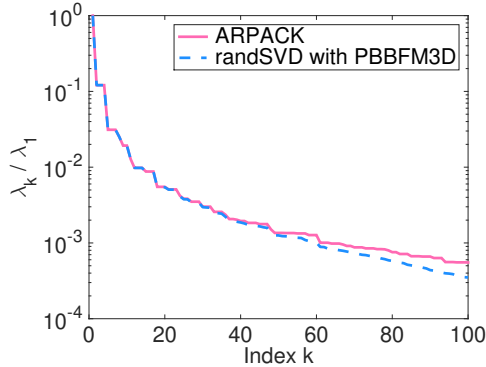


Figure 14: Decay in the first 100 eigenvalues (normalized) corresponding to the isotropic exponential covariance kernel $\exp(-r)$ with $n = 10^6$. “ARPACK” represents the reference eigenvalues. For randSVD, the input rank was 100 and the oversample parameter was 20. For PBBFMM3D, 32 cores were used and the parameters were: level = 5, interpolation order = 5, $\text{eps} = 10^{-5}$.

Lastly, we perform eigenvalue decomposition of the same covariance kernel $\exp(-r)$ on the 2D unit domain with unstructured grids [32] as shown in Figure 16. The eigenvectors were computed from randSVD accelerated by PBBFMM3D with a computation time of 172 seconds in average for 5 trials. Note that this 2D application is for illustration purpose and PBBFMM3D can handle 3D applications with similar computational complexity.

5. Conclusions

As the ability to generate data at large-scale increases, operations involving dense matrices has become computational bottlenecks in a wide range of applications. Therefore, it is essential to develop a package that is scalable, accurate, user-friendly, and easy to be adapted. In this paper, we presented our open-source software PBBFMM3D which computes the matrix-vector multiplication in linear time and memory, which is accelerated by OpenMP for shared memory machines, and which applies to all non-oscillatory smooth kernels. Our experimental results have verified its linear complexity, convergence, and parallel scalability. We have also discussed its broad applications and in particular, we showed a geostatistics application.

References

- [1] L. Greengard, V. Rokhlin, A fast algorithm for particle simulations, *Journal of computational physics* 73 (2) (1987) 325–348.

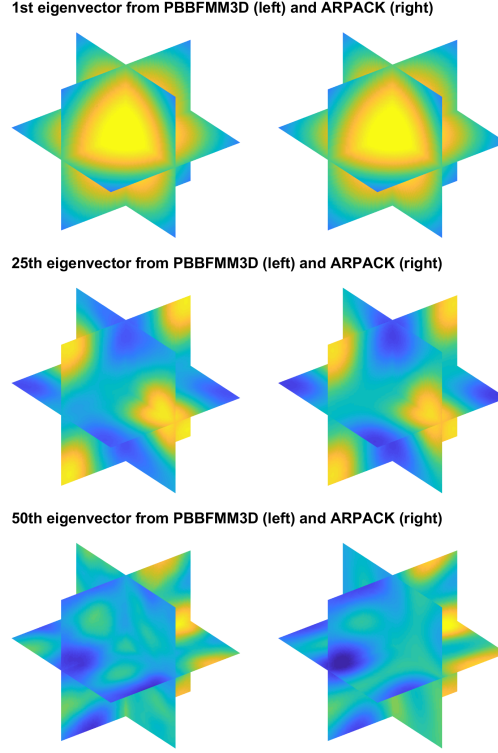


Figure 15: 1st, 25th, and 50th eigenvectors of the isotropic exponential covariance kernel $\exp(-r)$ with $n = 10^6$. “ARPACK” represents the reference eigenvectors and their pixel-wise RMSEs are 3.33×10^{-7} , 2.14×10^{-4} , and 5.78×10^{-4} , respectively.

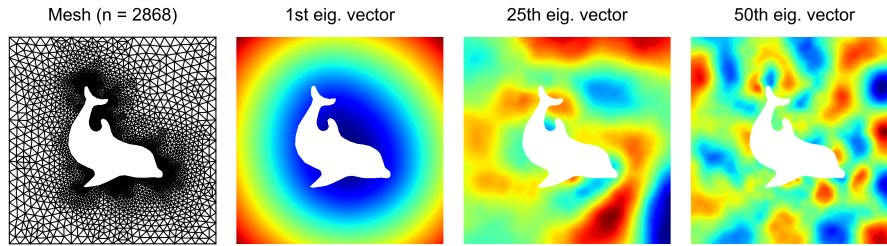


Figure 16: 2D unstructured grid with $n = 2,868$ for visualization purpose (left) and the 1st, 25th, and 50th eigenvectors of an isotropic exponential covariance kernel on the refined domain with $n = 693,888$. For PBBFMM3D, 32 cores were used and the parameters were: level = 5, interpolation order = 5, $\text{eps} = 10^{-5}$.

- [2] R. Simpson, Z. Liu, Acceleration of isogeometric boundary element analysis through a black-box fast multipole method, *Engineering Analysis with Boundary Elements* 66 (2016) 168–182.
- [3] C. Chen, S. Aubry, T. Oppelstrup, A. Arsenlis, E. Darve, Fast algorithms for evaluating the stress field of dislocation lines in anisotropic elastic media, *Modelling and Simulation in Materials Science and Engineering*.
- [4] A. G. Gray, A. W. Moore, N-body problems in statistical learning, in: *Advances in neural information processing systems*, 2001, pp. 521–527.
- [5] T. Hofmann, B. Schölkopf, A. J. Smola, Kernel methods in machine learning, *The annals of statistics* (2008) 1171–1220.
- [6] Y. Fu, K. J. Klimkowski, G. J. Rodin, E. Berger, J. C. Browne, J. K. Singer, R. A. Van De Geijn, K. S. Vemaganti, A fast solution method for three-dimensional many-particle problems of linear elasticity, *International Journal for Numerical Methods in Engineering* 42 (7) (1998) 1215–1229.
- [7] Y. Fu, G. J. Rodin, Fast solution method for three-dimensional Stokesian many-particle problems, *International Journal for Numerical Methods in Biomedical Engineering* 16 (2) (2000) 145–149.
- [8] L. F. Greengard, J. Huang, A new version of the fast multipole method for screened coulomb interactions in three dimensions, *Journal of Computational Physics* 180 (2) (2002) 642–658.
- [9] K.-i. Yoshida, N. Nishimura, S. Kobayashi, Application of fast multipole galerkin boundary integral equation method to elastostatic crack problems in 3d, *International Journal for Numerical Methods in Engineering* 50 (3) (2001) 525–547.
- [10] W. Fong, E. Darve, The black-box fast multipole method, *Journal of Computational Physics* 228 (23) (2009) 8712–8725.
- [11] L. N. Trefethen, *Approximation theory and approximation practice*, Siam, 2013.
- [12] J. Lee, A. Kokkinaki, P. K. Kitanidis, Fast large-scale joint inversion for deep aquifer characterization using pressure and heat tracer measurements, *Transport in Porous Media* 123 (2018) 533–543.

- [13] T. Takahashi, P. Coulier, E. Darve, Application of the inverse fast multipole method as a preconditioner in a 3D Helmholtz boundary element method, *Journal of Computational Physics* 341 (2017) 406–428.
- [14] Z. Gimbutas, V. Rokhlin, A generalized fast multipole method for nonoscillatory kernels, *SIAM Journal on Scientific Computing* 24 (3) (2003) 796–817.
- [15] A. Dutt, M. Gu, V. Rokhlin, Fast algorithms for polynomial interpolation, integration, and differentiation, *SIAM Journal on Numerical Analysis* 33 (5) (1996) 1689–1711.
- [16] C. R. Anderson, An implementation of the fast multipole method without multipoles, *SIAM Journal on Scientific and Statistical Computing* 13 (4) (1992) 923–947.
- [17] J. Makino, Yet another fast multipole method without multipoles-pseudoparticle multipole method, *Journal of Computational Physics* 151 (2) (1999) 910–920.
- [18] L. Ying, G. Biros, D. Zorin, A kernel-independent adaptive fast multipole algorithm in two and three dimensions, *Journal of Computational Physics* 196 (2) (2004) 591–626.
- [19] H. Cheng, Z. Gimbutas, P.-G. Martinsson, V. Rokhlin, On the compression of low rank matrices, *SIAM Journal on Scientific Computing* 26 (4) (2005) 1389–1404.
- [20] P.-G. Martinsson, V. Rokhlin, An accelerated kernel-independent fast multipole method in one dimension, *SIAM Journal on Scientific Computing* 29 (3) (2007) 1160–1178.
- [21] S. Rjasanow, Adaptive cross approximation of dense matrices, in: *Int. Association Boundary Element Methods Conf., IABEM, 2002*, pp. 28–30.
- [22] E. Agullo, B. Bramas, O. Coulaud, E. Darve, M. Messner, T. Takahashi, Task-based FMM for multicore architectures, *SIAM Journal on Scientific Computing* 36 (1) (2014) C66–C93.
- [23] E. Agullo, B. Bramas, O. Coulaud, E. Darve, M. Messner, T. Takahashi, Task-based FMM for heterogeneous architectures, *Concurrency and Computation: Practice and Experience* 28 (9) (2016) 2608–2629.

- [24] C. E. Rasmussen, C. K. I. Williams, Gaussian Processes for Machine Learning (Adaptive Computation and Machine Learning), The MIT Press, 2005.
- [25] M. L. Stein, Interpolation of spatial data : some theory for kriging, Springer series in statistics, Springer, New York, 1999.
- [26] P. K. Kitanidis, Introduction to geostatistics: applications in hydrogeology, Cambridge University Press, 1997.
- [27] D. S. Oliver, A. C. Reynolds, N. Liu, Inverse theory for petroleum reservoir characterization and history matching, Cambridge University Press, 2008.
- [28] T. Bui-Thanh, C. Burstedde, O. Ghattas, J. Martin, G. Stadler, L. C. Wilcox, Extreme-scale UQ for bayesian inverse problems governed by PDEs, in: SC '12: Proceedings of the International Conference on High Performance Computing, Networking, Storage and Analysis, 2012, pp. 1–11. doi:10.1109/SC.2012.56.
- [29] J. Lee, H. Yoon, P. K. Kitanidis, C. J. Werth, A. J. Valocchi, Scalable subsurface inverse modeling of huge data sets with an application to tracer concentration breakthrough data from magnetic resonance imaging, Water Resources Research 52 (7) (2016) 5213–5231.
- [30] A. K. Saibaba, J. Lee, P. K. Kitanidis, Randomized algorithms for generalized hermitian eigenvalue problems with application to computing karhunen–loève expansion, Numerical Linear Algebra with Applications 23 (2) (2016) 314–339.
- [31] N. Halko, P.-G. Martinsson, J. A. Tropp, Finding structure with randomness: Probabilistic algorithms for constructing approximate matrix decompositions, SIAM review 53 (2) (2011) 217–288.
- [32] M. S. Alnæs, J. Blechta, J. Hake, A. Johansson, B. Kehlet, A. Logg, C. Richardson, J. Ring, M. E. Rognes, G. N. Wells, The fenics project version 1.5, Archive of Numerical Software 3 (100). doi:10.11588/ans.2015.100.20553.